Quantifying the roles of bedrock damage and microclimate on potential soil production rates, erosion rates, and topographic steepness: A case study of the San Gabriel Mountains, California

Jon D. Pelletier

5 Department of Geosciences, University of Arizona, Gould-Simpson Building, 1040 East Fourth Street, Tucson, Arizona 85721-0077, USA

Correspondence to: Jon D. Pelletier (jdpellet@email.arizona.edu)

Abstract. Discerning how tectonic uplift rates, climate, soil production rates, erosion rates, and topography interact is essential for understanding the geomorphic evolution of mountain ranges. Perhaps the key independent variable in this

10 interaction is the potential soil production rate, i.e., the upper limit at which bedrock can be converted into transportable material. In this paper I document the controls on potential soil production rates using the San Gabriel Mountains (SGM) of California as a case study. The prevailing conceptual model for the geomorphic evolution of the SGM is that tectonic uplift rates control topographic steepness, erosion rates, and potential soil production rates. I test the alternative hypothesis that bedrock damage and microclimate also exert first-order controls on landscape evolution in the SGM via their influence on

15 potential soil production rates. I develop an empirical equation that relates potential soil production rates in the SGM to a bedrock damage index that depends on the local density of faults and a microclimatic index that relates to aspect-driven variations in vegetation cover and wildfire severity and frequency. Assuming a balance between soil production and erosion rates at the hillslope scale, I further show that observed trends in topographic steepness can be reproduced using the empirical equation for potential soil production rates. The results suggest that tectonic uplift rates, bedrock damage, and

20 microclimate play co-equal and interacting roles in controlling landscape evolution in the SGM and perhaps other tectonically active mountain ranges.

Keywords: soil production, cosmogenic radionuclides, bedrock damage, microclimate, San Gabriel Mountains

1 Introduction

25 The potential soil production rate (denoted herein by P_0) is the highest rate, achieved when soil cover is thin or absent, that bedrock or intact regolith can be converted into transportable material. Despite its fundamental importance, the geomorphic community has no widely accepted conceptual or mathematical model for potential soil production rates. Pelletier and Rasmussen (2009) took an initial step towards developing a model for potential soil production rates by relating P_0 values from granitic landscapes to mean annual precipitation and temperature values. The Pelletier and Rasmussen (2009)

model predicts P_0 values consistent with those reported in the literature from semi-arid climates, where P_0 values typically

range from ~30-300 m/Myr. In humid climates, the Pelletier and Rasmussen (2009) model predicts P_0 values greater than

1000 m/Myr (Fig. 2A of Pelletier and Rasmussen, 2009), which is broadly consistent with measured soil production rates of

up to 2500 m/Myr in the Southern Alps of New Zealand where mean annual precipitation (MAP) exceeds 10 m (Larsen et

5   al., 2014). The Pelletier and Rasmussen (2009) model was a useful first step, but clearly not all granites are the same. In

particular, variations in mineralogy (Hahm et al., 2014) and bedrock fracture density (Goodfellow et al., 2014) can result in

large variations in soil production rates in granites of the same climate. This study seeks to test the hypothesis that P_0 values

are controlled by bedrock damage and microclimate, and to explore how spatial variations in P_0 values drive variations in

erosion rates and topographic steepness.

10   The San Gabriel Mountains (SGM) of California (Fig. 1) have been the focus of many studies of the relationships

among tectonic uplift rates, climate, geology, topography, and erosion (e.g., Lifton and Chase, 1992; Spotila et al., 2002;

DiBiase et al., 2010; 2012; DiBiase and Whipple, 2011; Heimsath et al., 2012; Dixon et al., 2012). These studies take

advantage of a significant west-to-east gradient in exhumation rates in this range. What controls this gradient is debated.

Spotila et al. (2002) documented close associations among exhumation rates, mean annual precipitation (MAP) rates, and the

15   locations and densities of active tectonic structures. Spotila et al. (2002) concluded that landscape evolution in the SGM was

controlled by a combination of tectonics, climate, and bedrock characteristics. Heimsath et al. (2012) presented an alternative

view based on millennial-scale soil production and erosion rates. Heimsath et al. (2012) demonstrated that soil production

rates (P) and erosion rates (E) in rapidly eroding portions of the SGM greatly exceed P_0 values in slowly eroding portions of

the range. Assuming that climate and lithology are similar throughout the SGM, Heimsath et al. (2012) concluded that high

20   erosion rates, triggered by high tectonic uplift rates and the resulting steep topography, cause potential soil production rates

to increase, via a higher frequency of disturbance for a given soil thickness, above any limit set by climate and bedrock

characteristics.

Climate, lithology, and local fault density (which controls bedrock fracture density) vary greatly in the SGM (Fig.

1), however, with potentially important implications for potential soil production rates. Bedrock fracture density, which

25   controls the rate of bedrock breakdown into transportable material (e.g., Molnar et al., 2004; Koons et al., 2012; Goodfellow

et al., 2014), varies inversely with distance to individual faults and directly with fault density in the SGM (Chester et al., 2005; Savage and Brodsky, 2011). As such, it is reasonable to hypothesize that P_0 values are higher in the eastern and southern portions of the SGM in part because local fault density, and hence bedrock fracture density, is higher there. Mean annual precipitation (MAP) rates vary by a factor of two across the elevation gradient and exhibit a strong correlation with exhumation rates (Spotila et al., 2002, Fig. 10). In addition to this range-scale climate variation, slope aspect variations create microclimates in which vegetation cover and wildfire severity and frequency vary. Many steep, south-facing slopes of the SGM, for example, are chaparral shrublands (Holland, 1986) that are prone to frequent, high-severity wildfires (Keeley and Zedler, 2009) that these plant communities have evolved to use as a seed germination mechanism (Keeley, 1987). More wildfire-prone hillslopes experience faster rates of rock weathering compared to less wildfire-prone hillslopes (Blackwelder, 1927; Goudie et al., 1992; Dorn, 2003; Shtober-Zisu et al., 2010). In this paper I test the hypothesis that bedrock damage and microclimate exert first-order controls on potential soil production rates in the SGM. Further, I quantify the implications of this control on erosion rates and topographic steepness.

2 Data analysis and mathematical modeling

2.1 A model for potential soil production rates in the SGM

Soil buffers the underlying bedrock or intact regolith from physical weathering processes. P_0 values are a natural place to begin quantifying the coupled soil production-erosion system because they do not depend on soil thickness and its controlling factors; hence, they isolate the effects, if present, of environmental factors (e.g., water availability, vegetation cover, wildfire severity and frequency) and material factors (e.g., bedrock fracture density and lithology/mineralogy) that influence soil production rates. Moreover, P_0 values are the rate-limiting step for erosion in areas where deep-seated bedrock landsliding is not a dominant process. Slope failure in bedrock or intact regolith is common in fine-grained sedimentary rocks (e.g., Griffiths et al., 2004; Roering et al., 2005) but relatively uncommon in granitic terrain such as the SGM.

I calculated P_0 values (Supplementary Table 1) from the cosmogenically derived P values of Heimsath et al. (2012) using the exponential form of the soil production function:

$$P_{0,\text{meas}} = P e^{h/h_0} \tag{1}$$

where $P_{0,\text{meas}}$ refers to values inferred from measurements of P, h is soil thickness, and $h_0 = 0.32$ m for locations with $S \leq 30°$

and $h_0 = 0.37$ m for locations with $S > 30°$ based on the regressions reported in Figure 3 of Heimsath et al. (2012). Heimsath

et al. (2012) did not include data points from locations with no soil cover in their regressions because these data points

appear (especially for areas with $S > 30°$) to fit below the trend of equation (1). This implies that a humped production

function may be at work in the SGM. The mean value of P from areas with $S \leq 30°$ that lack soil cover is 183 m/Myr, i.e.,

slightly higher than, but within 2σ uncertainty of, the 170 ± 10 m/Myr value expected based on the exponential soil

production function fit by Heimsath et al. (2012). As such, it appears that for areas with $S \leq 30°$, data from locations with

and without soil cover are consistent with an exponential soil production function. The mean value of P from areas with $S >$

$30°$ that lack soil cover is 207 m/Myr, i.e., significantly lower than the 370 ± 40 m/Myr expected based on the exponential

soil production function. This suggests that a hump may exist in the soil production function for steep ($S > 30°$) slopes as

they transition to a bare (no soil cover) condition. To account for this, I estimated P_0 to be equal to $1.78P$ (i.e., the ratio of

370 to 207) at locations with $S > 30°$ that lack soil cover. This modification of equation (1) affects 4 of the 57 data points.

P_0 values estimated in this way can be modeled using the product of a coefficient c_1 (units of m/Myr) and

dimensionless indices related to bedrock damage, D, and microclimate, A:

$$P_{0,\text{pred}} = c_1 \cdot D \cdot A \tag{2}$$

where $P_{0,\text{pred}}$ refers to model predictions of P_0. The mathematical form of equation (2) honors trends between $P_{0,\text{meas}}$ and the

bedrock damage and microclimatic indices documented below.

The bedrock damage index D is based on the concept that soil production rates increase in bedrock that is more

pervasively fractured, together with the fact that bedrock fracture densities are correlated with the density of local faults

(Chester et al., 2005; Savage and Brodsky, 2011). Savage and Brodsky (2011) documented that bedrock fracture density

decreases as a power-law function of distance from small isolated faults, i.e. as $r^{-0.8}$ where r is the distance from the fault.

Fracture densities around larger faults and faults surrounded by secondary fault networks can be modeled as a superposition

of $r^{-0.8}$ decays from all fault strands (Savage and Brodsky, 2011). Chester et al. (2005) documented similar power-law

relationships between bedrock fracture density and local fault density in the SGM specifically. I define the bedrock damage

index D (Fig. 2A) as the sum of the inverse distances, raised to an exponent 0.8, from the point where the D value is being

computed to every pixel in the study area were a fault is located:

$$D = \sum_{\mathbf{x}'} \frac{\Delta x}{|\mathbf{x} - \mathbf{x}'|^{0.8}}$$ (3)

where Δx is the pixel width (included to make D dimensionless), x is the map location where bedrock damage is being

5   computed, and x' is the location of each mapped pixel in SGM where a fault exists. Equation (3) honors the roles of both the

distance to, and the density of, local faults documented by Savage and Brodsky (2011) because longer faults and/or more

mature fault zones with secondary fault zones have more pixels that contribute to the summation. A least-squares regression

of the logarithms of $P_{0,meas}$ to the logarithms of D (Fig. 3A) results in a p value of 0.014, indicating that the null hypothesis

that P_0 is unrelated to D can be rejected with 98.6% confidence.

10   The correlation between $P_{0,meas}$ and D values (Fig. 3A) is especially apparent at the extremes: 12 of 13 of the highest

$P_{0,meas}$ values come from locations where D is higher than the median value of 23, while the 7 lowest $P_{0,meas}$ values come

from areas where D is lower than the median value. The correlation between $P_{0,meas}$ and D values may include some

influence of lithology/mineralogy in addition to bedrock fracture density. For example, the high $P_{0,meas}$ values observed in the

Cloudburst summit and related monzogranites (Fig. 1) may be a function of their high biotite content in addition to their

15   proximity to locally dense fault networks. I attempted to introduce lithology as an additional variable but I found the number

of points in the dataset to be insufficient to objectively calibrate equation (2) separately to individual lithologies in addition

to bedrock damage and microclimate. There are several clusters of data points that weaken the correlation of $P_{0,meas}$ and D.

One such cluster is circled in Figures 1 and 3A. This cluster of five data points is located in an area with a relatively low

density of active faults (hence D values are low) but which nevertheless have relatively high P_0 values (155-261 m/Myr) and

20   thick soils (15-43 cm). These points are located in an area with an unusually high density of mapped landslides (Fig. 1). If

these five points were removed, the statistical significance of the relationship between P_0 and D would increase to 99.9% (p

= 0.001).

        A natural starting point for evaluating the climatic control on P_0 values in the SGM is to plot $P_{0,meas}$ values vs.

elevation, which is strongly correlated with MAP (Spotila et al., 2002). No systematic relationship between $P_{0,meas}$ values and

25   elevation exists (Fig. 4A). However, a relationship does exist between $P_{0,meas}$ values and $\cos(\varphi - \varphi_0)$, where φ is the slope

aspect (azimuth) and $\varphi_0 = \pi$ radians or 180° (included so that the value of $\cos(\varphi - \varphi_0)$ is maximized for south-facing slopes; $\varphi_0 = 0$ would maximize this function for north-facing slopes). As with the relationship between $P_{0,\mathrm{meas}}$ and D values, the relationship between $P_{0,\mathrm{meas}}$ and $\cos(\varphi - \varphi_0)$ is particularly apparent at the extremes, with the largest several values of $P_{0,\mathrm{meas}}$ occuring on south-facing hillslopes and the lowest several values occurring on north-facing hillslopes. Rather than using

5   slope aspect alone, microclimate is traditionally quantified using $S \cdot \cos(\varphi - \varphi_0)$, where S is the slope gradient (e.g., Callaway and Davis, 1983). The slope gradient is included in the standard microclimatic index to provide a continuous variation from steep south-facing slopes, where $S \cdot \cos(\varphi - \varphi_0)$ is close to 1 (if $S \approx 1$), to steep north-facing slopes, where $S \cdot \cos(\varphi - \varphi_0)$ is close to -1. In the absence of a slope gradient term, the index would change stepwise from maximum and minimum values among slopes that vary by only a degree or less (i.e., from a slope that dips slightly to the south to one that dips slightly to the

10   north). A least-squares regression of the logarithms of $P_{0,\mathrm{meas}}$ to A demonstrates that an approximately exponential relationship exists (i.e., a linear trend on a log-linear plot) for south-facing slopes ($p = 0.0003$ or >99.9% significance) (Fig. 3C):

$$A = \exp\left(c_2 S \cos(\varphi - \varphi_0)\right) \quad \text{if} \quad S \cos(\varphi - \varphi_0) > 0$$
$$= 1 \quad \text{if} \quad S \cos(\varphi - \varphi_0) \leq 0 \tag{4}$$

where $c_2 = 1.7 \pm 0.4$ is the best-fit value from the regression. A similar fit of $P_{0,\mathrm{meas}}$ to $S \cdot \cos(\varphi - \varphi_0)$ for north-facing slopes

15   indicates no relationship ($p = 0.5$), hence I used a constant value of $A = 1$ to honor the absence of a dependence of $P_{0,\mathrm{meas}}$ on $S \cdot \cos(\varphi - \varphi_0)$ for north-facing hillslopes. I propose that microclimate most likely controls P_0 values in the SGM as a result of the wildfire-prone nature of the chaparral shrublands (Keeley and Zedler, 2009), which tend to occur on steep, south-facing slopes (Holland, 1986), together with the fact that rock weathering rates tend to increase with wildfire severity and frequency (Blackwelder, 1927; Goudie et al., 1992; Dorn, 2003; Shtober-Zisu et al., 2010).

20   To constrain the mathematical form of the relationships among P_0, D, and A, I performed a multivariate linear regression of the logarithms of P_0 to the logarithms of both D and A. Transformed in this way, the best-fit coeffcients obtained by the regression are equivalent to the exponents of power-law relationships of P_0 (the dependent variable) to D and A (the independent variables). This regression yielded exponents of 1.1 ± 0.4 and 1.1 ± 0.3 for the relationship of P_0 to D and A, respectively. These values are sufficiently close to 1 that I chose to fix the values of the exponents to 1 (i.e., eqn. (2)) for

25   simplicity and reanalyze the data to determine the value of c_1 that yields the best fit of equation (2) to data. The result is $c_1 =$

6.7 m/Myr. The regression metrics of $\ln(P_{0,meas})$ vs. $\ln(P_{0,pred})$ are $R^2 = 0.24$ and $p = 10^{-4}$ (Fig. 3D). Equation (2), with $c_1 = 3.5$ m/Myr, also predicts P values (Fig. 4C, $R^2 = 0.41$, $p = 10^{-7}$).

2.2 Relating potential soil production rates to erosion rates and topographic steepness in the SGM

5   Equation (2), in combination with modified versions of equations (9)&(11) of Pelletier and Rasmussen (2009), i.e.,

$$P_0 e^{-h/h_0} = E \tag{5}$$

and

$$\frac{\kappa S}{1-(S/S_c)^2} = EL \ , \tag{6}$$

predict spatial variations in erosion rates and topographic steepness associated with spatial variations in bedrock damage and

10 microclimate predicted by equation (2). In equations (5)&(6), κ is a sediment transport coefficient (m^2/Myr) and L is a mean hillslope length (m). Equation (6) assumes a steady-state balance between soil production and erosion (modeled in eqn. (6) via the nonlinear slope-dependent model of Roering et al., 1999) at the hillslope scale.

        Spatial variations in erosion rates can be estimated using P_0 values predicted by equation (2) if spatial variations in soil thickness can also be determined. To do this, I developed an empirical relationship between soil thickness and slope

15 gradient derived from the Heimsath et al. (2012) dataset (Fig. 4D):

$$h = \frac{h_1}{S^b} \ , \tag{7}$$

with best-fit coefficients of $b = 1.0$ and $h_1 = 0.06$ m ($R^2 = 0.18$, $p = 0.001$). For this regression I shifted the soil thickness in areas with no soil upward to a small finite value (0.03 m). Without some shift, the 10 data points with $h = 0$ cannot be used, biasing the analysis towards areas with soil cover. The 0.03 m value was chosen because this is the minimum finite soil

20 thickness measured by Heimsath et al. (2012).

        Using equation (7) as a substitution, equations (5)&(6) can be combined to obtain a single equation that predicts topographic steepness, S:

$$\frac{S}{1-(S/S_c)^2} = \frac{L}{\kappa} P_{0,pred} \exp\left(-\frac{h_1}{h_0 S^b}\right) \tag{8}$$

Given a map of steepness obtained by solving equation (8), soil thicknesses and erosion rates can be mapped using equations (5) and (6), respectively.

Equations (5)&(6) are the same as equations (9)&(11) of Pelletier and Rasmussen (2009) except that their equation (9) included a term representing the bedrock-soil density contrast related to a slightly different definition of P_0 and their

5   equation (11) assumed a depth- and slope-dependent transport relation. Here I use a slope-dependent relation because depth-dependent models depend on the average soil depth *when soil is present* (because soil must be present for transport to occur), which cannot be determined for locations where soil thickness is currently zero.

The S values predicted by equation (8) (Fig. 2C) reproduce the observed first-order patterns of topographic steepness (Fig. 2D) if $L/\kappa = 0.003$ Myr/m and $S_c = 0.8$ are used. The value $S_c = 0.8$ was chosen because it is in the middle of

10   the range of values (i.e., 0.78-0.83) that Grieve et al. (2016) obtained for steep landscapes in California and Oregon. With this value for S_c, the best-fit value for L/κ was determined by minimizing the least-squares error between the model prediction (Fig. 2C) and observed variations in slope (Fig. 2D). Predicted and measured S values are lowest in the Western block and higher in the Sierra Madre, Tujunga, and Baldy blocks. The results in Figure 2 demonstrate that spatial variations in bedrock damage and microclimate can be directly associated with observed variations in topographic steepness in the

15   SGM. Soil thicknesses predicted by the model correlate inversely with slopes and P_0 values (Fig. 2E). Erosion rates (Fig. 2F) closely follow P_0 values, but they are lower in absolute value, reflecting the buffering effect of soil on bedrock physical weathering.

The absence of a systematic relationship between P_0 values and elevation (Fig. 4A) is perhaps surprising given the strong correlation Spotila et al. (2002) documented between exhumation rates, elevation, and MAP. Spotila et al. (2002)

20   cautioned, however, that this correlation could be coincidental as "prevailing winds happen to deliver the most precipitation along the southern range front where the most active structures are." The largest $P_{0,\text{meas}}$ values increase and then decrease with elevation between 1.5 and 2.5 km elevation, as indicated by the dashed curve that defines the envelope of the data in Figure 4A. The presence of two relatively large $P_{0,\text{meas}}$ values at low elevations in Figure 4A is a consequence of the influence of bedrock damage on P_0, since these locations are close to range-bounding faults and hence have large D values.

25   Mean canopy height, constrained from the Existing Vegetation Height layer of the U.S.G.S. LANDFIRE database (U.S.

Geological Survey, 2016), follows a similar pattern to that of $P_{0,meas}$ (Fig. 4B), correlating positively with elevation below 1.8

km a.s.l. and negatively with elevation above 1.8 km due to limited energy availability, especially in the cold-season months

when most precipitation falls in the SGM. Figures 4A&4B suggest that P_0 may have some dependence on range-scale

climate or vegetation. However, it is difficult to tease apart this possible control from other factors given the relatively

5   narrow range of elevations over which $P_{0,meas}$ values are available, i.e., 80% of the data points are from 1.6 to 2.2 km a.s.l.

3 Discussion

The key result of this paper is that statistically significant relationships exist between P_0 and both bedrock damage

(98.6% significance) and microclimate (>99.9% significance, for south-facing slopes). This result suggests that a revision to

10   the standard conceptual model for the relationships among tectonics, climate, potential soil production rates, and erosion

rates in the SGM may be necessary. I propose that the correlation between P_0 and E values documented by Heimsath et al.

(2012) can partly be understood as a consequence of the fact that E values are limited by (i.e., cannot exceed) P_0 values in

the relative absence of bedrock landsliding. This suggests that erosion rates in areas of thin or no soil are controlled by

potential soil production rates, not vice-versa. In addition, P_0 and E values tend to be correlated because they have similar

15   bioclimatic controls. The influence of wildfire on rock weathering rates, for example, has been documented in the field or

established experimentally by many authors (Blackwelder, 1927; Goudie et al., 1992; Dorn, 2003; Shtober-Zisu et al., 2010).

Similarly, wildfires alter rainfall-runoff partitioning in a way that tends to increase erosion rates, both on an event basis (e.g.,

Wagenbrenner and Robichaud, 2014) and over geologic time scales (Orem and Pelletier, 2016). Tectonic uplift rates still

exert significant control in this revised conceptual model, acting in concert with bedrock damage and microclimate, via their

20   control on soil thickness. Soil thickness is set by the difference between P_0 and E values. This difference tends to be smaller,

resulting in thinner soils and higher erosion rates, in areas of higher P_0 values because tectonic uplift tends be localized

where erosion rates (which correlate with potential soil production rates for the reasons stated above) are higher (e.g.,

Willett, 1999). This hypothesis is consistent with the inverse relationship between soil thickness and slope gradient (the latter

of which correlates with erosion rates, as documented by Heimsath et al. (2012), Figs. 1E&1F) documented in Figure 4D

25   together with the fact that the spatial variations in erosion rates predicted by the model (Fig. 2F) are similar to those

measured over million-year time scales (Spotila et al., 2002, Fig. 7B). The localization of tectonic uplift in areas of higher bedrock damage may also lead to enhanced localization of bedrock damage in a positive feedback. The higher variability of small-scale (i.e., 1-10 m) topographic curvature in areas of thin/patchy soil cover (Crouvi et al., 2013) may also be a factor in explaining the persistence of soil cover in rapidly eroding landscapes. Zones of locally high (positive) topographic curvature

5   may promote temporary soil deposition/storage not yet accounted for in most models of hillslope evolution. Channel steepness, which varies from west to east in a manner similar to P_0 values in the SGM (DiBiase et al., 2010), likely correlates with increasing P_0 values because tectonic uplift is localized where P_0 and E values are highest and because channels must steepen in areas of higher P_0 simply to remain bedrock channels, i.e., to transport the larger sediment fluxes delivered from hillslopes.

10   To the extent that the correlations documented in this paper are not stronger, it should be noted that substantial scatter is expected due to the inherent variability in P_0 values, which vary at the hillslope scale due to factors such as small-scale variations in bedrock characteristics. Equation (2) correctly predicts P_0 values to within a factor of 2 (the inherent range of variability at the hillslope scale estimated by Heimsath et al. (2012) in their Fig. 4A) for 72% of the dataset. Finally, the validity of this or any other model should not be judged exclusively on the strength of its correlations with data because

15   factors besides model quality, including the accuracy with which the independent variables (e.g., bedrock damage) can be quantified and the range of variation in the controlling variables captured by the dataset, factor into such correlations. While the fault map illustrated in Figure 1 represents a best attempt to map the fault network of the San Gabriel Mountains, a single missing fault strand, if located close to a cluster of cosmogenic sample locations, could significantly alter the relationship plotted in Figure 3A. The model of this paper may also improve as additional information becomes available on how best to

20   quantify the relationships among P_0 values, bedrock fracture density, and local fault density, and among P_0 values, vegetation cover, and wildfire severity and frequency. I also wish to stress that the mathematical forms of the relationships are not unique, and additional research in the SGM and elsewhere will almost certainly require a revision to the specific forms of the equations that relate P_0 values to bedrock damage and microclimate. My hope is that this paper stimulates the community to debate the factors that control potential soil production rates, better quantify the linkages among the potential

25   soil production rate and its controlling factors, and add to the remarkable datasets that Heimsath and his colleagues have

made available for studying the soil production problem. In particular, the analysis of this paper points to the need for measurements of soil production rates in the SCM and elsewhere across the broadest possible range of elevations, lithologies, and bedrock damage values.

5 **4 Conclusions**

In this paper I documented that bedrock damage (quantified using the local density of faults) and microclimate control potential soil production rates in the San Gabriel Mountains (SGM) of California. Assuming a balance between soil production and erosion rates at the hillslope scale, I further showed that observed trends in topographic steepness can be reproduced using the empirical equation for potential soil production rates based on bedrock damage and microclimate. The

10 results suggest co-equal and interacting roles for tectonic uplift rates, bedrock damage, and microclimate in the geomorphic evolution of the SGM. In this conceptual model, erosion rates increase in areas of where bedrock damage, microclimate, and potentially additional factors not explicitly account for here (e.g., mineralogy, large-scale variations in climate) make bedrock conducive to rapid soil production. The localization of tectonic uplift in areas of high erosion and potential soil production rates leads to a positive feedback in which erosion rates and factors conducive to soil production (e.g., high

15 bedrock damage values and severe, frequent wildfires) correlate and coevolve with potential soil production rates.

20

References

Blackwelder, E.: Fire as an agent in rock weathering, J. Geol., 35(2), 134–140, doi:10.1086/623392, 1927.

Callaway, R.M., and Davis, F.W.: Vegetation dynamics, fire, and the physical environment in coastal central California, Ecology, 74(5), 1567–1578, doi:10.2307/1940084, 1993.

Chester, J.S., Chester, F.M., and Kronenberg, A.K.: Fracture surface energy of the Punchbowl fault, San Andreas system, Nature, 437, 133–136, doi:10.1038/nature03942, 2005.

Crouvi, O., Pelletier, J.D., and Rasmussen, C.: Predicting the thickness and aeolian fraction of soils in upland watersheds of the Mojave Desert, Geoderma, 195-196C, 94-110, doi:10.1016/j.geoderma.2012.11.015, 2013.

5   DiBiase, R.A., Whipple, K.X., and Heimsath, A.M.: Landscape form and millennial erosion rates in the San Gabriel Mountains, CA, Earth Planet. Sci. Lett., 289(1-2), 134–144, doi:10.1016/j.epsl.2009.10.036, 2010.

DiBiase, R.A. and Whipple, K.X.: The influence of erosion thresholds and runoff variability on the relationships among topography, climate, and erosion rate, J. Geophys. Res. Earth Surf., 116, F04036, doi:10.1029/2011JF002095, 2011.

DiBiase, R.A., Heimsath, A.M., and Whipple, K.X.: Hillslope response to tectonic forcing in threshold landscapes, Earth
10   Surf. Process. Landf., 37, 855–865, doi:10.1002/esp.3205, 2012.

Dixon, J.L., Hartshorn, A.S., Heimsath, A.M., DiBiase, R.A., and Whipple, K.X.: Chemical weathering response to tectonic forcing: A soils perspective from the San Gabriel Mountains, California, Earth Planet. Sci. Lett., 323, 40–49, doi:10.1016/j.epsl.2012.01.010, 2012.

Dorn, R.I.: Boulder weathering and erosion associated with a wildfire, Sierra Ancha Mountains, Arizona, Geomorphology,
15   55, 155–171, doi:10.1016/S0169-555X(03)00138-7, 2003.

Goodfellow, B.W., Skelton, A., Martel, S.J., Stroeven, A.P., Jansson, K.N., and Hättestrand, C.: Controls of tor formation, Cairngorm Mountains, Scotland, J. Geophys. Res. Earth Surf., 119, 225–246, doi:10.1002/2013JF002862, 2014.

Goudie, A.S., Allison, R.J. and McLaren, S.J.: The relations between modulus of elasticity and temperature in the context of the experimental simulation of rock weathering by fire, Earth Surf. Process. Landf.,17, 605–615, doi:
20   10.1002/esp.3290170606, 1992.

Grieve, S.W.D., Mudd, S.M., Hurst, M.D., and Milodowski, D.T.: A nondimensional framework for exploring the relief structure of landscapes, Earth Surf. Dynam., 4, 309–325, doi:10.5194/esurf-4-309-2016, 2016.

Griffiths, P.G., Webb, R.H., and Melis, T.S.: Frequency and initiation of debris flows in Grand Canyon, Arizona, J. Geophys. Res., 109, F04002, doi:10.1029/2003JF000077, 2004.
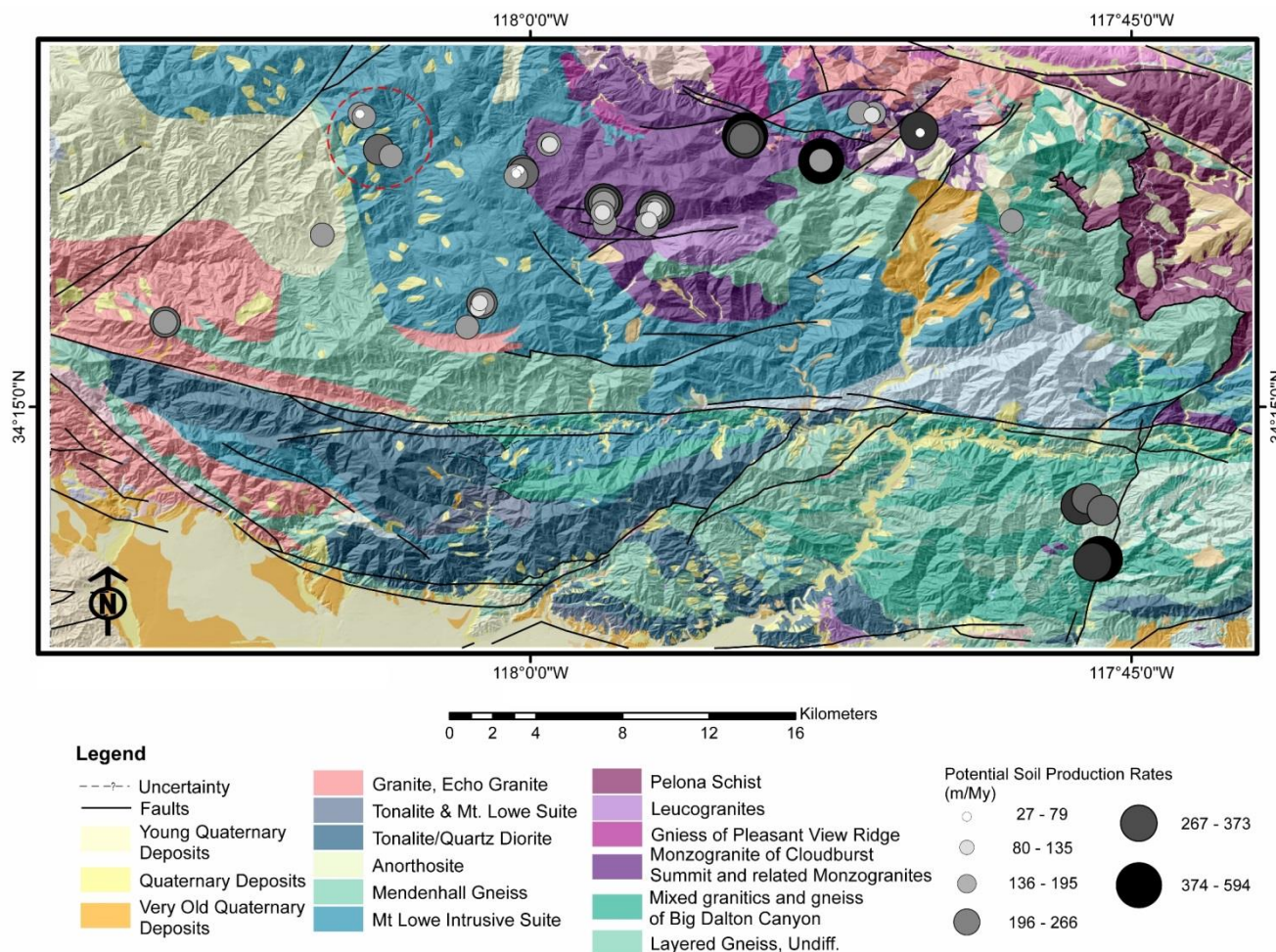
12

Hahm W.J., Riebe, C.S., Lukens, C.E., Araki, S.: Bedrock composition regulates mountain ecosystems and landscape evolution, Proc. Nat. Acad. Sci. USA, 111, 3207–3212. doi:10.1073/pnas.1315667111, 2014.

Heimsath, A.M., DiBiase, R.A., and Whipple, K.X.: Soil production limits and the transition to bedrock dominated landscapes, Nature Geosci., 5, 210–214, doi:10.1038/NGEO1380, 2012.

5 Holland, R.F.: Preliminary descriptions of the terrestrial natural communities of California, State of California, The Resources Agency, Nongame Heritage Program, Dept. Fish & Game, Sacramento, Calif. 156 pp., 1986.

Keeley, J.E.: Role of fire in seed germination of woody taxa in California Chaparral, Ecology, 68(2), 434-443, doi: 10.2307/1939275, 1987.

Keeley, J.E, and Zedler, P.H.: Large, high-intensity fire events in southern California shrublands: debunking the fine-grain
10   age patch model, Ecol. Appl., 19(1), 69–94, doi:10.1890/08-0281.1, 2009.

Koons, P.O., Upton, P., and Barker, A.D., The influence of mechanical properties on the link   between   tectonic   and topographic evolution, Geomorphology, 137(1), 168–180, doi:10.1016/j.geomorph.2010.11.012, 2012.

Larsen, I.J., Almond, P.C., Eger, A., Stone, J.O., Montgomery, D.R., and Malcolm, B.: Rapid soil production and weathering in the Southern Alps, New Zealand, Science, 343(6171), 637–640, doi:10.1126/science.1244908, 2014.

15 Lifton N.A., and Chase, C.G.: Tectonic, climatic and lithologic influences on landscape fractal dimension and hypsometry: implications for landscape evolution in the San Gabriel Mountains, California, Geomorphology, 5(1-2), 77–114, doi:10.1016/0169-555X(92)90059-W, 1992.

Molnar, P., Anderson, R.S., and Anderson, S.P.: Tectonics, fracturing of rock, and erosion, J. Geophys. Res. Earth Surf., v. 112, F03014, doi:10.1029/2005JF000433, 2007.

20 Morton, D.M., and Miller, F.K.: Preliminary Geologic Map of the San Bernardino 30'x60' Quadrangle, California, v. 1.0, U.S. Geological Survey Open-File Report 03-293, Reston, Virginia, 2003.

Nourse, J.A.: Middle Miocene reconstruction of the central and eastern San Gabriel Mountains, southern California, with implications for evolution of the San Gabriel fault and Los Angeles basin, in Barth, A., ed., Contributions to the Crustal Evolution of the Southwestern United States: Boulder, Colorado, Geological Society of America Special
25   Paper 365, 161–185, 2002.

Orem, C.A., and Pelletier, J.D.: The predominance of post-wildfire erosion in the long-term denudation of the Valles Caldera, New Mexico, J. Geophys. Res. Earth Surf., 121, 843–864, doi:10.1002/2015JF003663, 2016.

Pelletier, J.D., and Rasmussen, C.: Quantifying the climatic and tectonic controls on hillslope steepness and erosion rate, Lithosphere, 1(2), 73–80, doi:10.1130/L3.1, 2009.

5 Roering, J.J., Kirchner, J.W., and Dietrich, W.E.: Evidence for nonlinear, diffusive sediment transport on hillslopes and implications for landscape morphology, Water Resour. Res., 35(3), 853–870, doi:10.1029/1998WR900090, 1999.

Roering, J.J., Kirchner, J.W., and Dietrich, W.E.: Characterizing structural and lithologic controls on deep-seated landsliding: Implications for topographic relief and landscape evolution in the Oregon Coast Range, USA, Geol. Soc. Am. Bull., 117(5/6), 654–668, doi:10.1130/B25567.1, 2005.

10 Savage, H.M., and Brodsky, E.E.: Collateral damage: Evolution with displacement of fracture distribution and secondary fault strands in fault damage zones, J. Geophys. Res., 116, B03405, doi:10.1029/2010JB007665, 2011.

Shtober-Zisu, N., Tessler, N., Tsatskin, A., and Greenbaum, N.: Accelerated weathering of carbonate rocks following the 2010 wildfire on Mount Carmel, Israel, Int. J. Wildland Fire, 24, 1154–1167, doi:10.1071/WF14221, 2015.

Spotila, J.A., House, M.A., Blythe, A.E., Niemi, N.A., and Bank, G.C.: Controls on the erosion and geomorphic evolution of
15 the San Bernardino and San Gabriel Mountains, southern California, in Barth, A., ed., Contributions to Crustal Evolution of the Southwestern United States: Boulder, Colorado, Geological Society of America Special Paper 365, 205–230, 2002.

U.S. Geological Survey: LANDFIRE database, digital data available at http://www.landfire.gov/, accessed July 5, 2016.

U.S. Geological Survey and California Geological Survey: Quaternary fault and fold database for the United States, digital
20 data available at http//earthquakes.usgs.gov/regional/qfaults/, accessed July 5, 2016.

Wagenbrenner, J.W. and Robichaud, P.R.: Post-fire bedload sediment delivery across spatial scales in the interior western United States, Earth Surf. Process. Landforms, 39, 865–876. doi:10.1002/esp.3488, 2014.

Willett, S.D.: Orogeny and orography: The effects of erosion on the structure of mountain belts, J. Geophys. Res., 104(B12), 28,957–28,981, doi:10.1029/1999JB900248, 1999.

Yerkes, R.F. and Campbell, R.H.: Preliminary Geologic Map of the Los Angeles 30'x60' Quadrangle, Southern California,

v. 1.0, U.S. Geological Society Open-File Report 2005-1019, Reston, Virginia, 2005.

Figure 1. Geologic map of the central San Gabriel Mountains, California. Potential soil production rates inferred from the data of Heimsath et al. (2012) are also shown. Lithologic units were compiled using Yerkes and Campbell (2005), Morton and Miller (2003), and Figure 3 of Nourse (2002). Faults were mapped from Morton and Miller (2003) and the Quaternary fault and fold database of the United States (U.S. Geological Survey and California Geological Survey, 2006). The dashed red circle identifies a cluster of data points discussed in Section 2.1.
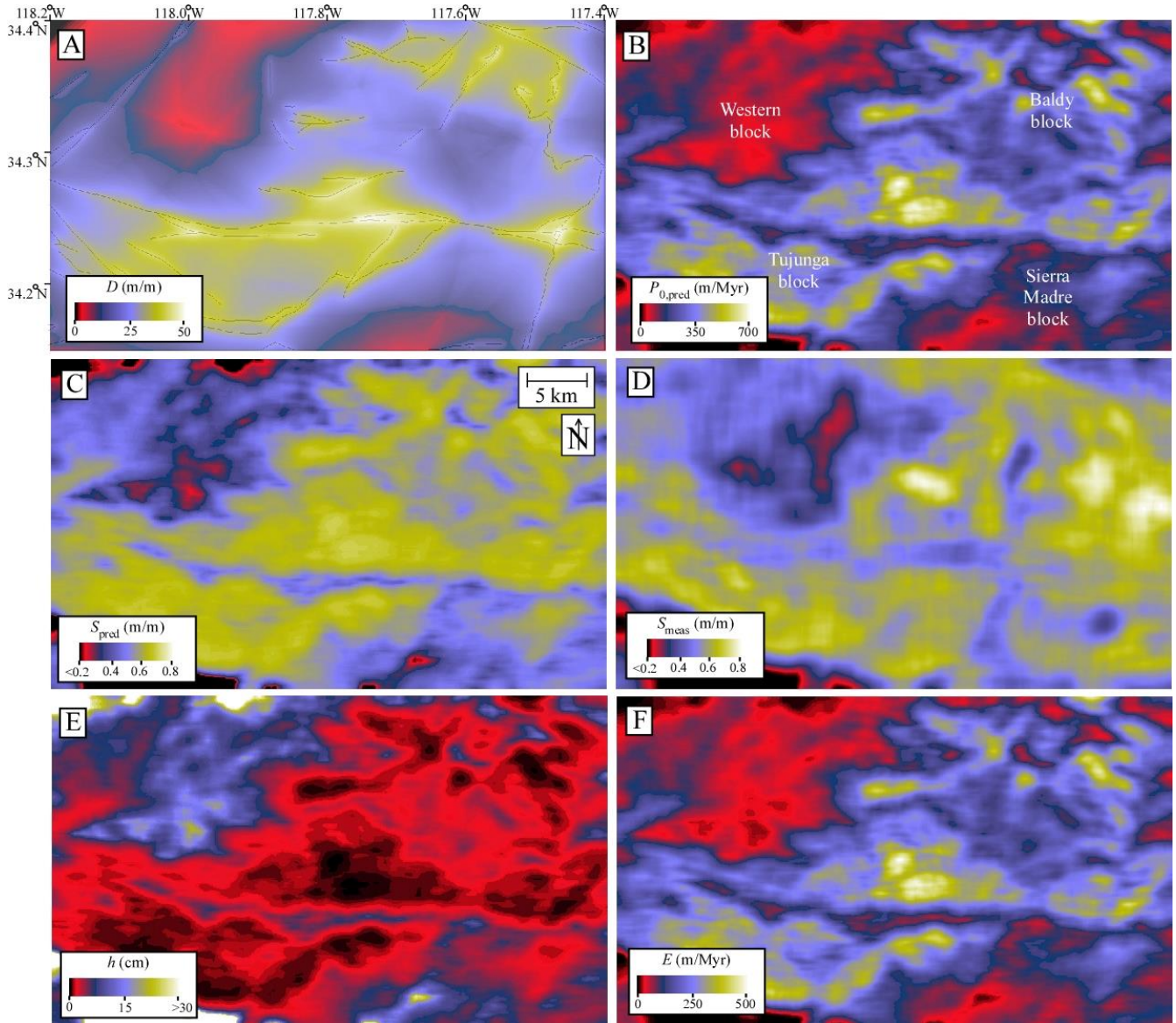
Figure 2. Color maps illustrating spatial variations of the damage index (*D*), potential soil production rate (*P*₀), predicted and observed values of slope gradient, *S*, soil thickness, *h*, and erosion rate, *E*. (A) Color map of damage index *D* (eqn. (3)) with fault traces superimposed. (B) Color map of *P*₀ values estimated as described in Section 2.1. (C) Color map of *S* values predicted by equations (7)&(8), smoothed by a moving average filter with a 1-km length scale to emphasize patterns at the landscape scale. (D) Color map of measured *S* values, smoothed in the same manner as (C). (E) Color map of soil thicknesses, *h*. (F) Color map of erosion rates, *E*.
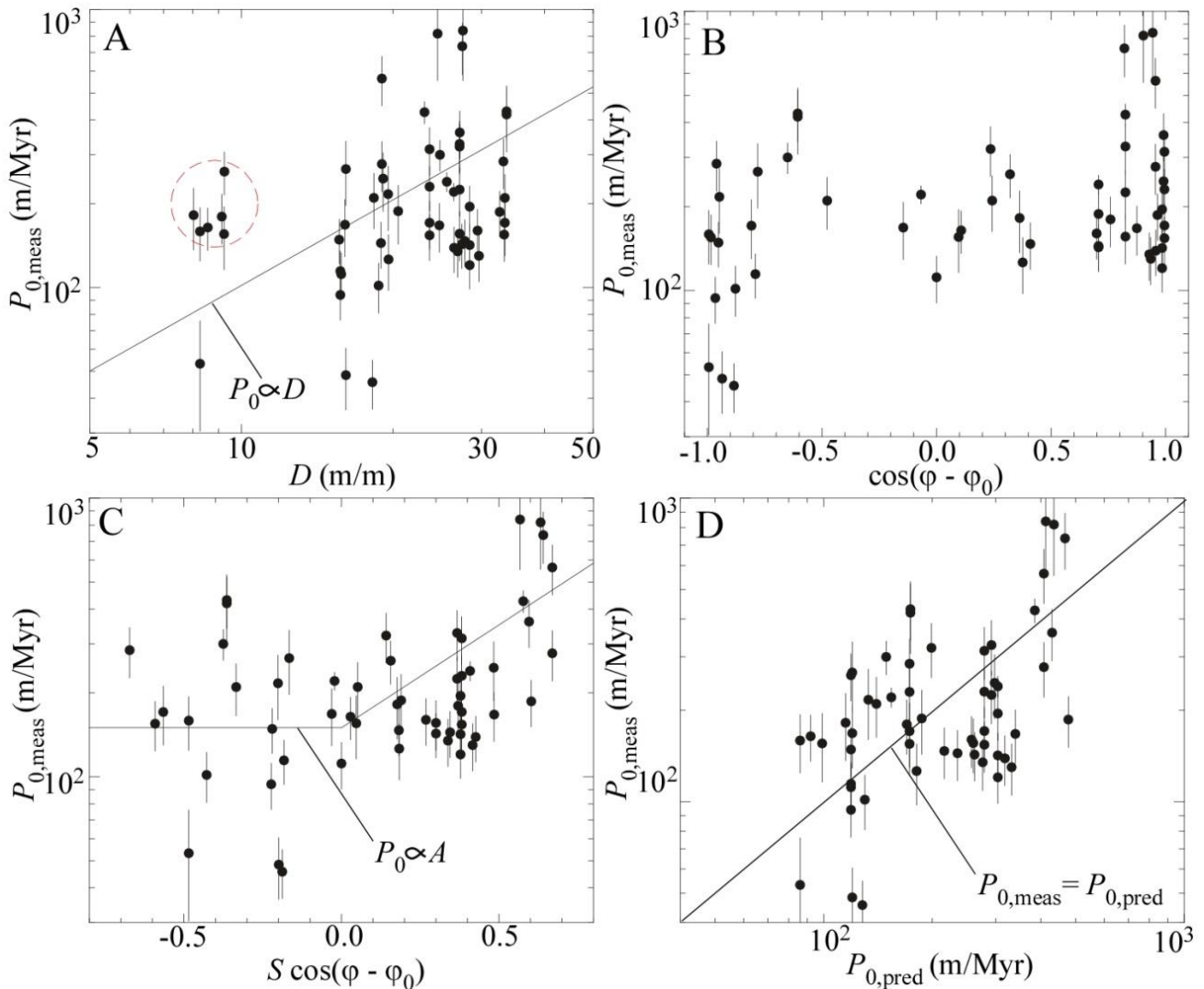
16

Figure 3. Plots of P_0 and their relationship to the bedrock damage and microclimatic indices. (A) Plot of measured potential soil production rates, $P_{0,meas}$, versus bedrock damage index, D. The red dashed circle refers to the cluster of data points discussed in Section 2.1. (B) Plot of $P_{0,meas}$ versus $\cos(\varphi - \varphi_0)$. (C) Plot of $P_{0,meas}$ versus $S \cdot \cos(\varphi - \varphi_0)$. Linear relationship between P_0 and A also shown. (C) Plot of measured versus predicted P_0 values.

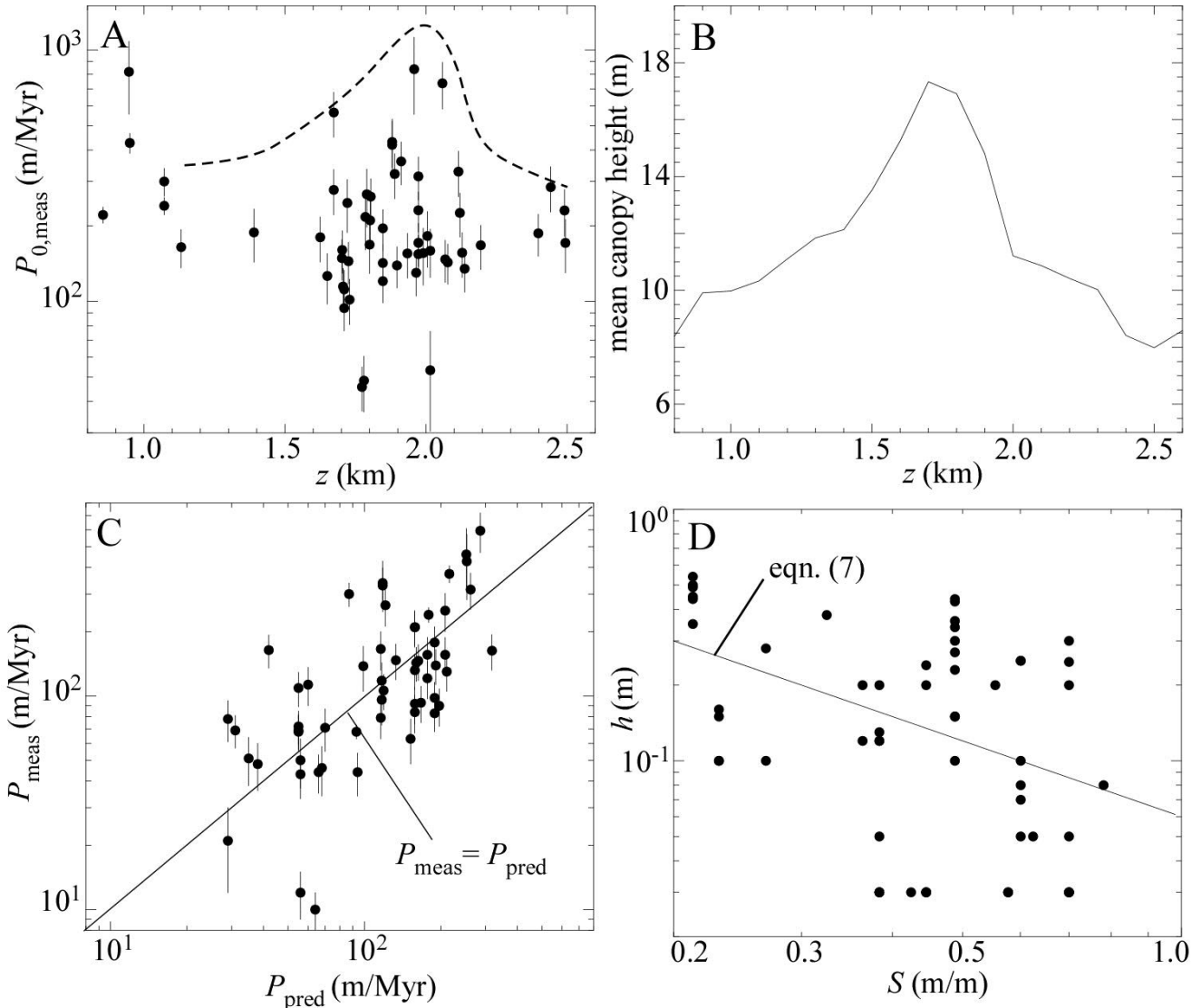Earth **Surface**
Dynamics
Discussions

Figure 4. (A) Plot of $P_{0,meas}$ versus elevation, z. The dashed curve identifies the maximum values or "envelope" of the data. (B) Plot of mean canopy height versus elevation using the U.S. Geological Survey LANDFIRE database. (C) Plot of measured versus predicted values for the soil production rate, P. The predicted value is from equation (2) with $c_1 = 3.5$ m/Myr. (D) Plot of soil thickness, h, versus slope gradient, S. Results of the linear regression of the logarithms of h and S also shown.